


## Unveiling the pressure-driven metal-semiconductor-metal transition in the doped $TiS_2$

Jiajun Chen(陈佳骏), Xindeng Lv(吕心邓), Simin Li(李思敏), Yaqian Dan(但雅倩), Yanping Huang(黄艳萍), Tian Cui(崔田)

**Citation:**Chin. Phys. B, 2024, 33 (**6**): 067104. DOI: 10.1088/1674-1056/ad4325
Journal homepage: http://cpb.iphy.ac.cn; http://iopscience.iop.org/cpb

**What follows is a list of articles you may be interested in**

---

## Magnetism, heat capacity, magnetocaloric effect, and magneto-transport properties of heavy fermion antiferromagnet CeGaSi

Li-Bo Zhang(张黎博), Qing-Xin Dong(董庆新), Jian-Li Bai(白建利), Qiao-Yu Liu(刘乔宇), Jing-Wen Cheng(程靖雯), Cun-Dong Li(李存东), Pin-Yu Liu(刘品宇), Ying-Rui Sun(孙英睿), Yu Huang(黄宇), Zhi-An Ren(任治安), and Gen-Fu Chen(陈根富)
Chin. Phys. B, 2024, 33 (**6**): 067101. DOI: 10.1088/1674-1056/ad3060

## Pressure- and temperature-dependent luminescence from $Tm^{3+}$ ions doped in $GdYTaO_4$

Peng-Yu Zhou(周鹏宇), Xiu-Ming Dou(窦秀明), Bao-Quan Sun(孙宝权), Ren-Qin Dou(窦仁琴), Qing-Li Zhang(张庆礼), Bao Liu(刘鲍), Pu-Geng Hou(侯朴赓), Kai-Lin Chi(迟凯邺), and Kun Ding(丁琨)
Chin. Phys. B, 2022, 31 (**1**): 017101. DOI: 10.1088/1674-1056/ac0526

## First-principles study of electronic structure and magnetic properties of $Sr_3Fe_2O_5$ oxide

Mavlanjan Rahman(买吾兰江·热合曼) and Jiuyang He(何久洋)
Chin. Phys. B, 2021, 30 (**11**): 117107. DOI: 10.1088/1674-1056/abfa06

## The role of CALYPSO in the discovery of high-$T_c$ hydrogen-rich superconductors

Wenwen Cui(崔文文), Yinwei Li(李印威)
Chin. Phys. B, 2019, 28 (**10**): 107104. DOI: 10.1088/1674-1056/ab4253

## First-principles study of the elastic and thermodynamic properties of thorium hydrides at high pressure

Xiao-Lin Zhang(张晓林), Yuan-Yuan Wu(武媛媛), Xiao-Hong Shao(邵晓红), Yong Lu(鲁勇), Ping Zhang(张平)
Chin. Phys. B, 2016, 25 (**5**): 057102. DOI: 10.1088/1674-1056/25/5/057102

---

**RAPID COMMUNICATION**

# Unveiling the pressure-driven metal–semiconductor–metal transition in the doped $TiS_2$

Jiajun Chen(陈佳骏)[1], Xindeng Lv(吕心邓)[1], Simin Li(李思敏)[1], Yaqian Dan(但雅倩)[1], Yanping Huang(黄艳萍)[1,†], and Tian Cui(崔田)[1,2,‡]

[1] *Institute of High Pressure Physics, School of Physical Science and Technology, Ningbo University, Ningbo* 315211, *China*
[2] *State Key Laboratory of Superhard Materials, College of Physics, Jilin University, Changchun* 130012, *China*

(Received 13 February 2024; revised manuscript received 18 April 2024; accepted manuscript online 25 April 2024)

Conventional theories expect that materials under pressure exhibit expanded valence and conduction bands, leading to increased electrical conductivity. Here, we report the electrical properties of the doped 1*T*-$TiS_2$ under high pressure by electrical resistance investigations, synchrotron x-ray diffraction, Raman scattering and theoretical calculations. Up to 70 GPa, an unusual metal–semiconductor–metal transition occurs. Our first-principles calculations suggest that the observed anti-Wilson transition from metal to semiconductor at 17 GPa is due to the electron localization induced by the intercalated Ti atoms. This electron localization is attributed to the strengthened coupling between the doped Ti atoms and S atoms, and the Anderson localization arising from the disordered intercalation. At pressures exceeding 30.5 GPa, the doped $TiS_2$ undergoes a re-metallization transition initiated by a crystal structure phase transition. We assign the most probable space group as $P2_12_12_1$. Our findings suggest that materials probably will eventually undergo the Wilson transition when subjected to sufficient pressure.

**Keywords:** high pressure, transition metal dichalcogenides, doped $TiS_2$, electronic phase transition

**PACS:** 71.30.+h, 62.50.–p, 07.35.+k, 64.60.–i **DOI:** 10.1088/1674-1056/ad4325

## 1. Introduction

The exploration of anomalous anti-Wilson transitions, shifting from metallic to nonmetallic states in fundamental electronic systems under extreme pressures, is pivotal for probing the complex physical processes associated with the electronic configurations of materials. Traditional assumptions posit that heightened pressure should broaden the valence and conduction bands, theoretically favoring increased electrical conductivity. Yet, the actual responses of some materials under extreme conditions deviate from these theoretical projections, particularly in the case of alkali metals such as sodium (Na) and lithium (Li), which serve as prominent examples.[1,2] This trend of unconventional transitions is echoed in recent studies on transition metal dichalcogenides (TMDs), such as the restacked $TaS_2$.[3] It is evident that the anti-Wilson phase transitions in metals and TMDs materials unfold through different underlying mechanisms, in metals, it is often linked to the displacement of core electrons to interstitial spaces within the lattice, whereas in TMDs, the transitions are more commonly associated with shifts between layers.

Within the TMDs family, $TiS_2$ stands out for its notable discrepancies between theoretical expectations and experimental findings.[4] The crystalline structure of stoichiometric $TiS_2$ is composed of a single triatomic sheet of titanium atoms, which is sandwiched between two layers of sulfur atoms bonded together covalently. These [S–Ti–S] layers are stacked together through van der Waals forces, forming a quasi-two-dimensional structure.[4] As expected, it shares the same *P*-3*m*1 space group under ambient pressure, similar to 1*T*-$TaS_2$ and 1*T*-$TiSe_2$.[5] Initially, $TiS_2$ was believed to be a semiconductor based on early photochemical and theoretical calculation studies.[6,7] However, coupled with the electrical transport experiments conducted by Thompson *et al.* collectively suggest that $TiS_2$ displays metallic behavior.[8] Recent years have brought a growing body of evidence, especially from terahertz spectroscopy and scanning tunneling microscopy (STM) studies,[4,9] confirming that the intrinsic property of $TiS_2$ is to behave fundamentally as a semiconductor. The observed metallic behavior in experiments is attributed to doping from an excess of Ti atoms.[10] Undoubtedly, the stoichiometric $TiS_2$ model does not accurately represent real $TiS_2$ materials. A more experimentally precise depiction would involve a doping model including Ti interstitials. These raise expectations for the emergence of novel phenomena in $TiS_2$ under high-pressure conditions.

In this work, we have meticulously carried out *in-situ* electrical transport measurements, x-ray diffraction (XRD), and Raman spectroscopy on the doped $TiS_2$ under high-pressure conditions. To complement these experimental methods, we also conducted first-principles calculations using a self-intercalation layer model, aiming to thoroughly understand the material's behavior when compressed. The

†Corresponding author. E-mail: huangyanping@nbu.edu.cn
‡Corresponding author. E-mail: cuitian@nbu.edu.cn

© 2024 Chinese Physical Society and IOP Publishing Ltd 

resistivity–temperature ($R$–$T$) profile at the initial pressure point unambiguously exhibits the sample's metallic nature. Intriguingly, our electrical transport measurements reveal an unusual pressure-induced metal–semiconductor–metal transition. The detection of the Sh peak in our Raman spectra confirms the anticipated presence of interlayer Ti atoms in our sample. Our first-principles calculations indicate that the anti-Wilson transition from metal to semiconductor observed at 17 GPa is attributed to intercalated Ti atoms. This results from the promoted electron localization by the intercalating Ti atoms and the disorder of these atoms, leading to Anderson localization. The re-metallization transition occurred at pressures exceeding 30.5 GPa is probably because of the crystal structure phase transition.

## 2. Experimental methods and computational details

The powder employed in this study was procured from Mukenano, showcasing an impressive purity of 99.99%. We utilized a diamond anvil cell (DAC) as our pressure generating device, with tungsten sheets serving as sealing gaskets. In order to calibrate the pressure, a ruby with a diameter of approximately 3 μm was positioned within the chamber. High-pressure electrical resistance measurements were conducted in a nonmagnetic DAC made of BeCu alloy, using a standard four-electrode method. The XRD experiment was performed at the BL15U1 beamline of Shanghai Synchrotron Radiation Facility (SSRF) with a wavelength of 0.6199 Å. For the Raman experiment, we employed a backscattering geometry for measurement using an incident laser wavelength of 532 nm on the MonoVista CRS$^3$ system.

Structural relaxations and electronic properties were carried out using density functional theory (DFT) with the Perdew–Burke–Ernzerhof (PBE) of generalized gradient approximation (GGA), as implemented in the Vienna *ab initio* simulation package (VASP) code. The ion–electron were described using the all-electron projector augmented wave (PAW) method with $4s^2 3d^2$, and $3s^2 3p^4$ as valence electrons for Ti and S, respectively. To obtain a better energy convergence, we have chosen a plane-wave cutoff energy of 400 eV and Monkhorst–Pack $k$-meshes of $2\pi \times 0.02^{-1}$ to ensure that the enthalpy converges to less than 1 meV/atom. The crystalline orbital Hamiltonian population (COHP) and integrated crystalline orbital Hamiltonian population (ICOHP) were calculated using LOBSTER code which digests electronic-structure output from VASP.

## 3. Results and discussion

To explore the electrical transport properties of the doped 1$T$-$TiS_2$ under high pressure, we conducted *in situ* electrical transport measurements at low temperature, as shown in Fig. 1. At the starting pressure of 0.8 GPa, it exhibits metallic behavior. A noteworthy reduction in the resistance was observed as the pressure increased to 9.2 GPa. This phenomenon was complemented by evidence indicating an increase in carrier concentration, as demonstrated in the Hall measurement conducted by Liu Bao *et al.*[11] However, it is noted that the upturn in resistance occurs at lower temperature with further compression, which represents the progressive transformation of the doped $TiS_2$ into a semiconductor. In addition, the region of semiconducting properties rapidly expands with increasing pressure, reaching a semiconductor-like behavior in the whole temperature range at 17 GPa and the value of resistance reaches maximum at 23 GPa. As the pressure continues to increase, the semiconducting behavior and overall resistance start to decrease. Beyond 30.5 GPa, a new metallic behavior gradually emerges with rising pressure, and remains consistent up to the maximum pressure recorded in our measurement, as depicted in Figs. 1(c) and 1(d). The unexpected pressure-induced transition from metal–semiconductor–metal within such a range of pressure has rarely been detected in TMDs before.

Excluding the metal–semiconductor–metal transition, a convex hull is observed around 215 K below 12.2 GPa. This phenomenon is probably ascribed to the short-range ordered charge density wave (CDW) patterns, which are linked to the electron doping induced by additional Ti atoms.[12–14] Therefore, we consider this convex hull to represent a CDW-like pattern. This is similar to the long-range ordered CDW observed in other TMDs materials such as $TaS_2$ and $TiSe_2$, where the size of the bulges also decreases with increasing pressure.[15,16] Figure 1(a) demonstrates that CDW-like state is obvious near ambient pressure, as the pressure increases, the convex hull is suppressed and disappears at 13.2 GPa. After the semiconductor transition is completed, the CDW-like convex hull re-emergences prominently on the temperature-resistance curve when the pressure is increased to 21 GPa. This pressure-induced CDW-like phenomenon has also been presented in other TMDs and TMDs-related materials, such as $MoS_2$ and $SnSe_2$.[17–19] The present CDW in low-dimensional system raises the question whether these transitions are primarily driven by the instability in the electronic subsystem, the vibrational subsystem, or a combination of both. Herein, further research is necessary to explore the reemergence of CDW-like state in the doped $TiS_2$.

Alterations in crystallographic phases frequently induce modifications in the electronic structure. Given this circumstance, we performed *in situ* x-ray diffraction (XRD) measurements at elevated pressures. The obtained XRD spectra reveal the presence of distinctive peaks of the sample, with an additional dim tungsten peak denoted by a star. Upon comparison with the standard XRD spectra of the sample, it is noted that the tungsten peak distinctly differs from the characteris-

tic peaks of the sample, exhibiting a measurable displacement. Consequently, this separation ensures that the presence of the tungsten peak does not interfere with the analysis of the experimental data. The Rietveld refinement of the powder XRD pattern at 0.5 GPa confirms the presence of the trigonal $P$-3$m$1 phase, as depicted in Fig. 2(b). This analysis yields lattice parameters of $a = b = 3.405(4)$ Å and $c = 5.700(3)$ Å, with excellent agreement with previous report,[7] evident from the profile matching parameters $R_{wp} = 1.49\%$ and $R_p = 0.79\%$. Synchrotron XRD patterns were obtained up to 71.6 GPa, and selected patterns are shown in Fig. 2(a). With increasing pressure, all peaks gradually shift towards the larger angle. At a pressure of 28.1 GPa, we detected a distinctive peak at approximately 11.6°, and its intensity increases with pressure, signaling a pressure-driven phase transition. Comparing our high pressure XRD to the theoretical structure proposed in previous study,[20,21] we found that they do not align. The orthorhombic $P2_12_12_1$ space group, supported by its Pawley fitting with experimental data showing profile matching parameters $R_{wp} = 0.30\%$ and $R_p = 0.23\%$ as in Fig. 2(c), provides the most consistent model of Ti doped $TiS_2$ under high pressure. Furthermore, our electronic measurement reveals a semiconductor–to–metal transition at 30.5 GPa, closely aligned with the observed phase transition at 28.1 GPa. This correlation suggests that the crystal structure transition instigates the metallization in the doped $TiS_2$.

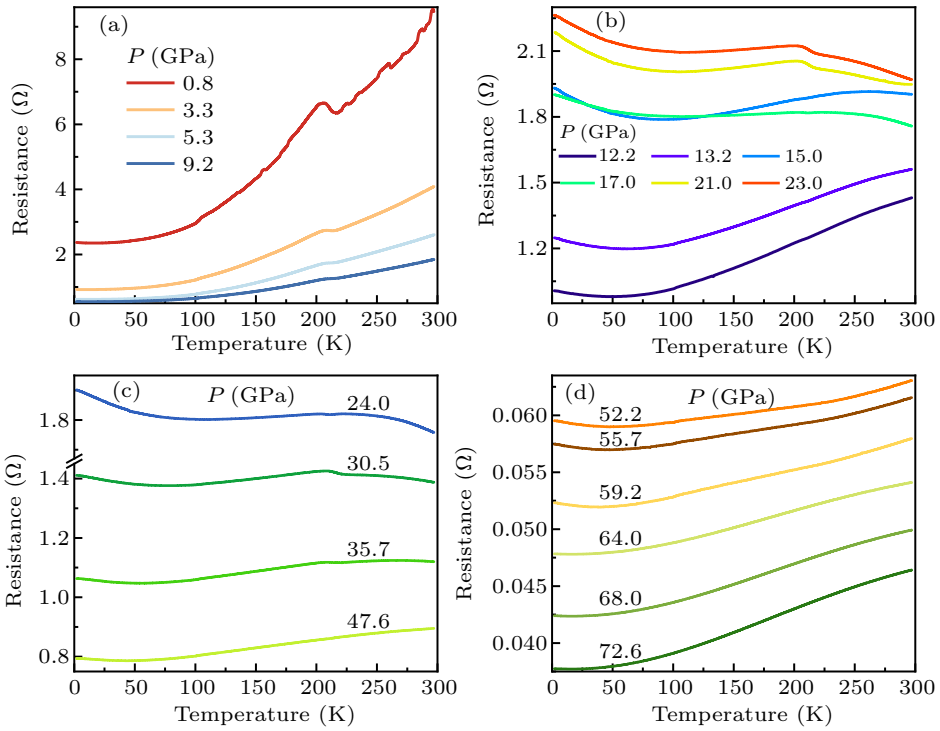



**Fig. 1.** Temperature dependent electrical resistance of the doped 1$T$-$TiS_2$ in the pressure range of (a) 0.8–9.2 GPa, (b) 12.2–23.0 GPa, (c) 24.0–47.6 GPa, and (d) 52.2–72.6 GPa.

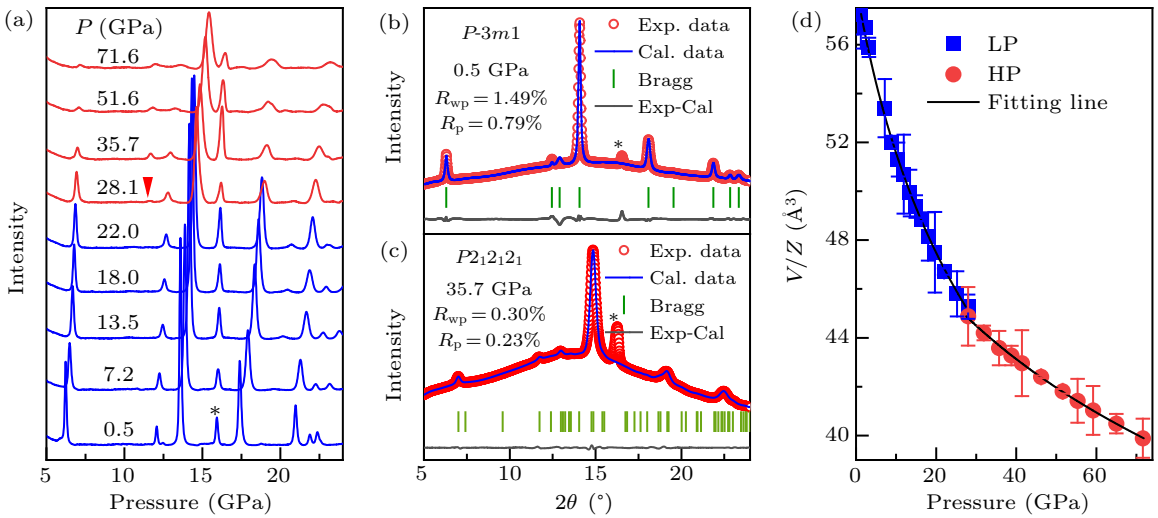



**Fig. 2.** (a) Angle-dispersive XRD patterns for the doped $TiS_2$ at selected pressures at room temperature ($\lambda = 0.6199$ Å), the triangle marks the new diffraction peak belonging to the high pressure phase. (b) and (c) Representative refinements of the patterns collected at 0.5 GPa and 35.7 GPa. (d) The pressure dependence of volume obtained from the experimental data.

Raman scattering is acknowledged as a direct technique for observing alterations in phono modes. We conducted *in-situ* high pressure Raman spectroscopy measurement on the doped 1*T*-$TiS_2$ to elucidate the metal–semiconductor–metal transition. The ambient phase comprises a primitive cell with three atoms, giving rise to nine phonon modes at the Brillouin zone point. The symmetries of these modes can be effectively represented by the irreducible representations[22]

$$\Gamma = E_u + E_g + A_{1g} + A_{2u}.$$

The Raman spectrum is characterized by the presence of $A_{1g}$ and $E_g$ modes, which are Raman active, while $A_{2u}$ and $E_u$ modes are active in infrared region. The Raman spectrum under ambient pressure is shown in Fig. 3(a), which is similar to that of $TiSe_2$.[23] We identified a prominent mode at 350 $cm^{-1}$ alongside a less intense mode at 240 $cm^{-1}$. In contrast to $TiSe_2$, the doped $TiS_2$ exhibits an additional peak adjacent to the $A_{1g}$ mode, known as Sh peak, a distinctive shoulder peak. This Sh peak is notably influenced by strong interlayer correlation, both an increase in the number of layers and the intercalation of additional metal atoms between layers directly affect the shape of the Sh peak.[24–26] The inset in Fig. 3(a) shows that the wavenumber of the Sh peak shifts almost in lockstep with the $A_{1g}$ peak, supporting that the Sh peak is not an independent feature but rather a broadening of the $A_{1g}$ peak due to interlayer doping effects. In the studies of Konrad *et al.* and Barajas *et al.*, it was directly suggested that the Sh peak results from phonon splitting caused by interstitial Ti atoms inserted between layers.[4,26] Evidently, the presence of the Sh peak indicates that our sample is not an ideal $TiS_2$. To fully account for the anomalous phenomena observed in electrical testing, our investigations must proceed on the basis of an interstitial insertion model.

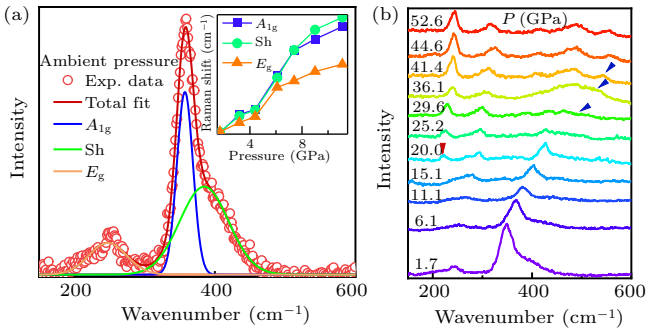



**Fig. 3.** (a) Raman spectra of the doped $TiS_2$ at ambient pressure, the micrograph illustrates the pressure induced Raman shifts of peak $A_{1g}$, peak $E_g$ and peak Sh. (b) Raman patterns of the doped $TiS_2$ ranging from 0 GPa to 52.6 GPa, the inverted triangles and stars indicate the new peaks.

Figure 3(b) displays the evolution of Raman spectrum under pressure, revealing a blue shift of all peaks as the pressure increases. Notably, a new peak emerges at the wavenumber of 218 $cm^{-1}$ at the pressure of 20 GPa, which is within the characteristic range of 200 $cm^{-1}$ to 300 $cm^{-1}$, typically associated with S–S bonds, suggesting that the applied pressure induces the sulfur atoms to draw nearer to each other, consequently leading to the formation of S–S bonds. This phenomenon is also observed in high-pressure Raman studies of $TiSe_2$, attributed to the strengthening of pressure-induced Se–Se interactions.[23] The Raman spectra measurements further verify the pressure-induced evolution of the structure at the pressure of 28.1 GPa. In Fig. 3(b), a convex hull is observed around 520 $cm^{-1}$ under the pressure of 29.6 GPa, and continues to increase with the pressure increasing. These findings provide consistent evidence with XRD data. Therefore, electrical measurement, XRD diffraction and Raman experiments all provide consistent evidence for the high pressure semiconductor–metal phase transition.

Upon analyzing the Raman spectral data, the full width at half maximum (FWHM) of the peaks was determined for pressures up to 11.1 GPa, as shown in Fig. S2a. Under these conditions, an anomalous broadening of the Sh peak was evident under increased pressure. As the pressure exceeded 11.2 GPa, the task of differentiating between the $A_{1g}$ symmetry peak and the Sh peak became increasingly arduous. This effect was pronounced at 25.2 GPa, where the Sh peak's profile merged indiscernibly with that of the $A_{1g}$ peak, as depicted in Fig. S2b. The broadening of the $A_{1g}$ vibrational mode observed in $TiS_2$ is attributed to the enhanced coupling between interlayer Ti atoms and intralayer atoms under high-pressure conditions. This coupling intensification reflects the significant pressure-induced modifications in the lattice vibrational interactions, indicative of the complex interplay between the Ti atoms across the different layers of the material. Such phenomena are critical to understanding the modifications in the electronic and crystallographic architectures that may arise, particularly as they pertain to the potential emergence of new phases or the stabilization of charge density wave states under extreme conditions. The pronounced CDW-like hump observed in the *R*–*T* curves between 21 GPa and 36 GPa is likely a manifestation of this cause.

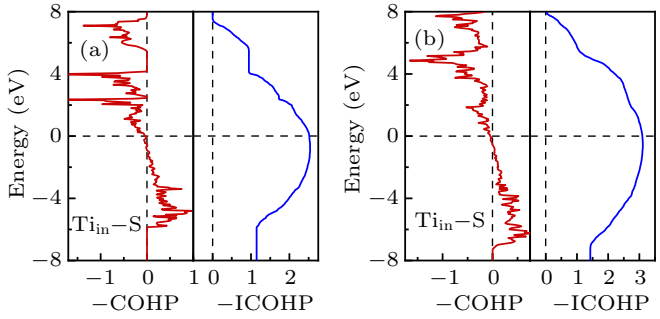



**Fig. 4.** The calculated crystalline orbital Hamiltonian population (−COHP, left panel) and integrated crystalline orbital Hamiltonian population (−ICOHP, right panel) of the doped $TiS_2$ at 0 GPa (a) and 20 GPa (b).

In particular, in order to explore the impact of intercalated Ti atoms on electronic properties of $TiS_2$ under high pressure, we proposed a potential crystal structure with an excess ratio of 1/16 intercalated Ti atoms, as shown in Fig. S3. The intercalated Ti atoms are positioned midway between adjacent layers

of Ti atoms. The Ti self-intercalation in $TiS_2$ introduces a considerable degree of unpredictability and disorder. To explore the mechanisms underlying the anomalous electrical transport properties, we expanded the unit cell and optimized the structure while preserving the original crystallographic framework and parameters. We qualitatively investigated the origins of the observed transport anomalies from metal to semiconductor. We obtained crystal orbital Hamilton population (COHP) at ambient pressure and 20 GPa, respectively. As shown in Figs. 4(a) and 4(b), the intercalating Ti atoms form bonds with adjacent S atoms at both ambient pressure and 20 GPa. Moreover, the integrals of –COHP (–ICOHP) up to $E_F$ is 2.5 at ambient pressure, and change to 3.1 at 20 GPa. This suggests that the intercalating Ti atoms and their adjacent S atom counterparts undergo an enhanced coupling, thus promoting the electron localization around the intercalating Ti atoms. On the other hand, the disorder of the intercalating Ti atoms can also lead to Anderson localization. Compared to the metallic characteristics in pristine $TiS_2$ within this pressure range, it is reasonable to conclude that the intercalating Ti atoms are the primary factor causing the transition from metal to semiconductor.

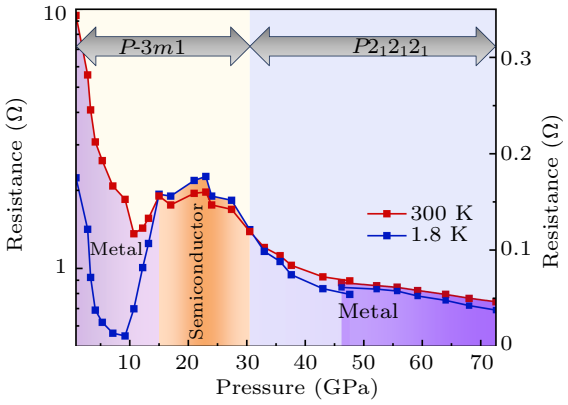



**Fig. 5.** Phase transition diagram of the doped $TiS_2$ under pressure, and the resistance at temperatures of 300 K and 1.8 K at different pressures. First run of measurement from 0.8 GPa to 47.6 GPa (left coordinate axis), second run of measurement from 46.2 GPa to 72.6 GPa (right coordinate axis).

## 4. Conclusions

In conclusion, we have executed a comprehensive investigation of the electrical transport properties and structural transformations of the doped $TiS_2$ under high pressure. Our findings contribute a distinctive case to the TMDs, wherein we observed a sequence of transitions: from metal to semiconductor, then back to metal. The metal–semiconductor transition is induced by the augmented coupling of doped Ti atoms with neighboring sulfur atoms under pressure, coupled with the Anderson localization in this disordered system. The reentrant metallization, manifesting post 30.5 GPa, is ascribed to a structure phase transition. This research reveals a scenario in which the intricate electronic structure induces an anti-Wilson transition. Under sufficiently high pressure, this transition reverts to a Wilson transition, ultimately leading to a metallic state.

## Acknowledgements

The authors thank the staff of the BL15U1 beamline of Shanghai Synchrotron Radiation Facility (SSRF). This work was supported by the National Natural Science Foundation of China (Grant No. 12304072), Program for Science and Technology Innovation Team in Zhejiang (Grant No. 2021R01004), and Natural Science Foundation of Ningbo (Grant No. 2021J121). This work was also supported by the User Experiment Assist System of Shanghai Synchrotron Radiation Facility (SSRF).

## References

[1] Ma Y, Eremets M, Oganov A R, Xie Y, Trojan I, Medvedev S, Lyakhov A O, Valle M and Prakapenka V 2009 *Nature* **458** 182
[2] Bergara A, Neaton J B and Ashcroft N W 2000 *Phys. Rev. B* **62** 8494
[3] Dong Q, Pan J, Li S, Li C, Lin T, Liu B, Liu R, Li Q, Huang F and Liu B 2023 *J. Am. Chem. Soc.* **145** 14581
[4] Barajas-Aguilar A H, Garay-Tapia A, Strupiechonski E, Justo-Guerrero M A, Santos-Cruz J and Jiménez-Sandoval S 2023 *Adv. Theory Simul.* **6** 2200821
[5] Pal B, Cao Y, Liu X, Wen F, Kareev M, N'Diaye A T, Shafer P, Arenholz E and Chakhalian J 2019 *Sci. Rep.* **9** 1896
[6] Greenaway D L and Nitsche R 1965 *J. Phys. Chem. Solids* **26** 1445
[7] Allan D R, Kelsey A A, Clark S J, Angel R J and Ackland G J 1998 *Phys. Rev. B* **57** 5106
[8] Thompson A H 1975 *Rev. Lett.* **35** 1786
[9] Wang H, Qiu Z, Xia W, Ming C, Han Y, Cao L, Lu J, Zhang P, Zhang S, Xu H and Sun Y Y 2019 *J. Phys. Chem. Lett.* **10** 6996
[10] Zhao Y, Cai W, Fang Y, Ao H, Zhu Y and Qian Y 2019 *ChemElectroChem* **6** 2231
[11] Liu B, Yang J, Han Y, Hu T, Ren W, Liu C, Ma Y and Gao C 2011 *J. Appl. Phys.* **109** 053717
[12] Van Bakel G P E M and De Hosson J T M 1992 *Phys. Rev. B* **46** 2001
[13] Li S, Dong Q, Feng J, Wang Y, Hou M, Deng W, Susilo R A, Li N, Dong H, Wan S, Gao C and Chen B 2021 *Inorg. Chem.* **60** 7857
[14] Martino E, Pisoni A, Ćirić L, Arakcheeva A, Berger H, Akrap A, Putzke C, Moll P J W, Batistić I, Tutiš E, Forró L and Semeniuk K 2020 *NPJ 2D Mater. Appl.* **4** 7
[15] Webb A W, Feldman J L, Skelton E F, Towle L C, Liu C Y and Spain I L 1976 *J. Phys. Chem. Solids* **37** 329
[16] Chi Z H, Zhao X M, Zhang H, Goncharov A F, Lobanov S S, Kagayama T, Sakata M and Chen X J 2014 *Phys. Rev. Lett.* **113** 036802
[17] Ying J, Paudyal H, Heil C, Chen X J, Struzhkin V V and Margine E R 2018 *Phys. Rev. Lett.* **121** 027003
[18] Yu Y G and Ross N L 2011 *J. Phys.: Condens. Matter* **23** 055401
[19] Zhou D, Xu Y, Bai L, Shen B, Wang X, Zou Y and Tian J 2018 *J. Alloys Compd.* **757** 448
[20] Tang X F, Zhu S X, Liu H, Zhang C, Wu Q Y, Liu Z T, Song J J, Guo X, Wang Y S, Ma H, Zhao Y Z, Wu F Y, Liu S Y, Liu K H, Yuan Y H, Huang H, He J, Xu W, Liu H Y, Duan Y X and Meng J Q 2022 *Chin. Phys. B* **31** 037103
[21] Rajaji V, Janaky S, Sarma S C, Peter S C and Narayana C 2019 *J. Phys.: Condens. Matter* **31** 165401
[22] Unger W K, Reyes J M, Singh O, Curzon A E 1978 *Solid State Commun.* **28** 109
[23] Sandoval S J, Chen X K and Irwin J C 1992 *Phys. Rev. B* **45** 14347
[24] Li D, Qin X Y and Gu Y J 2006 *Mater. Res. Bull.* **41** 282
[25] Sherrell P C, Sharda K, Grotta C, Ranalli J, Sokolikova M S, Pesci F M, Palczynski P, Bemmer V L and Mattevi C 2018 *ACS Omega* **3** 8655
[26] Wilczyński K, Gertych A P and Zdrojek M 2023 *J. Phys. Chem. C* **127** 20870